Development of microstructures in rapidly-quenched Mg85Y9Zn6 alloy ribbons during heating at a constant speed examined by simultaneous small- and wide angle scattering measurements

AUTHOR(S):

Okuda, Hiroshi; Tanaka, Hiroto; Shiratake, Takahiro; Yamasaki, Michiaki; Kawamura, Yoshihito

CITATION:

Okuda, Hiroshi ...[et al]. Development of microstructures in rapidly-quenched Mg85Y9Zn6 alloy ribbons during heating at a constant speed examined by simultaneous small- and wide angle scattering measurements. Acta Materialia 2016, 118: 95-99

ISSUE DATE:

2016-10-01

URL:

http://hdl.handle.net/2433/261195

Development of microstructures in rapidly-quenched $Mg_{85}Y_9Zn_6$ alloy ribbons during heating at a constant speed examined by simultaneous small- and wide angle scattering measurements

Hiroshi Okuda, Hiroto Tanaka, Takahiro Shiratake, Michiaki Yamasaki, Yoshihito Kawamura

Department of materials science and engineering, Kyoto University, Sakyo-ku Kyoto 606-8501.

Magnesium Research Center, Kumamoto University, Kurokami, Kumamoto 860-8555

Abstract

Developments of microstructures during heating $Mg_{85}Y_9Zn_6$ amorphous ribbons have been examined by in-situ synchrotron radiation small- and wide- angle scattering measurements. The samples show sharp crystallization peak in a DSC measurement at 450 K for a heating rate of 10K/min. During and just after crystallization, clustering occurred first within supersaturated hcp crystallites, with concomitant hcp grain growth. Above 550 K, the spatial arrangements of the cluster became anisotropic, eventually lead to 18R LPSO structures accompanied by introduction of stacking faults.

Key words:

Long-period stacking ordered structures (LPSO), Mg-Y-Zn, Small-and wide-angle X-ray scattering (SWAXS),

- Corresponding author
  okuda.hiroshi.5a@kyoto-u.ac.jp
  +81-75-753-5193

Final manuscript(accepted)　Publication：
Acta Materialia 118（2016）95-99.　http://dx.doi.org/10.1016/j.actamat.2016.06.028

Introduction

Mg-Y-Zn ternary alloys form a series of phases called long-period stacking ordered structures (LPSO). [1-6] Three stable periodicities of 10H, 14H and 18R are reported in the alloy system, which can be treated as phases.[6-10] Intensive works have been made to understand the atomistic structures by electron microscopy[2,5,6,11,12] and X-ray diffraction [13], as well as theoretical examination using first principle calculations[14-16]. For the LPSO structures in Mg-Y-Zn ternary alloys, experimental works revealed that the periodicity of the concentration modulation is well-defined[1-6,11,12] but the position of the clusters in the segregated layer is rather flexible[10,13,17,18], i.e., the alloy does not behave as a chemical compound having well-defined atomic positions. Recent pubications suggest that the so-called $L1_2$ clusters in the LPSO structures[19] contain an interstitial atom at the body-center position of the $L1_2$ Y_8Zn_6 clusters, i.e., the actual composition of the clusters may Y_8Zn_6M where M can either be Mg or Zn, which is not fully determined yet. For simplicity, we call the cluster $L1_2$ clusters in the following discussion. Then, questions, why and how this happens, becomes important not only because of basic knowledge in phase transformation theory and alloy phase stability, but also because these fluctuation in the structure may also affect analysis and interpretations of many properties like thermal conductivity, elastic moduli, deformation mechanism and so on.

Therefore, it is important to understand the phase transformation kinetics in the alloy system to control the microstructure. Understanding of the phase transformation kinetics is also very useful to test models used in the computational materials design.

So far, a standard approach in precipitation /phase transformation study, i.e., a solution treatment-quench-annealing procedure works only for dilute alloy composition in the present alloy system, since the phase boundary of LPSO phase, for example, 18R structure in MgYZn is known to contact directly with liquid phase[9,10,20], and therefore it is hard to obtain largely supersaturated solid solution by quenching from solid. To answer the question if the initial stage of phase transformation to form LPSO is controlled by instability of order parameters such as spinodal decomposition[21-23], and if so, how, we need to realize a supersaturated solid solution for a concentrated composition, for example, that for 18R. In the present work, we demonstrate a structural evolution of the sample rapidly quenched from liquid having a nominal composition of $Mg_{85}Y_9Zn_6$, during heating the sample at a constant speed of 10 K/min using in-situ and simultaneous small- and wide- angle scattering measurements.

Experimental

The alloy ribbons with a nominal composition of $Mg_{85}Y_9Zn_6$ have been rapidly quenched from melt by a Cu single roll rotating at a speed of 50 m/s in Ar atmosphere. Ribbon samples were amorphous in the as melt-quenched state. A calorimetric result obtained by a differential scanning calorimeter (DSC) at a heating rate of 10 K/min. is shown in Fig.1. A sharp exothermic peak corresponding to crystallization of the amorphous ribbon was observed at 448 K, and at higher temperatures between 520 K and 590 K, another diffuse peak was detected. No macroscopic precipitation or phase separation were found by SEM/EPMA micrographs for as melt-spun samples. The in-situ simultaneous small- and wide- angle scattering measurements were performed at the beam line 6A of Photon Factory, KEK Tsukuba with a photon energy of 8.2 keV and the beam line 45XU of Spring8, Sayo Japan with a photon energy of 12.4 keV. The samples were sealed with carbon films and were kept in a furnace in a sample chamber evacuated by a turbo molecular pump. Figure 2 gives a schematic illustration of the in-situ small- and wide angle X-ray scattering (SWAXS) measurements. The sample chamber has a large port connected to SAXS path, and two sets of WAXS windows, one with smaller angle for 12.4 keV and the other for larger angle for 8.2 keV. SAXS measurements were made with a Pilatus 1M(R) or a Pilatus 2M(R), and WAXS measurements were made with a Pilatus 100K(R). The samples were heated at a heating rate of 10 K/min, the same speed as that for calorimetric measurements.

Results and Discussions

Figure 3 (a) and (b) give SAXS profiles during heating around and above the crystallization temperature, Tx, respectively. Even below the crystallization temperature of 448 K, the SAXS profiles show a well-defined shoulder component between the magnitude of the scattering vector, q=5 nm^{-1} and 8 nm^{-1}, that slightly increased with increasing temperatures although the SAXS intensity of as melt-quenched samples is negligibly small. This means that aggregation of very small clusters started to occur even in amorphous region, when the sample temperature becomes high enough to allow atomic motion for aggregation of a couple of solute atoms. The temperatures where such clustering was observed by SAXS profile was fond to be above the temperature where weak endothermic reaction by relaxation was observed in Fig.1.

It should be noted that this strong tendency of aggregation of solute atoms is an important feature related to spinodal decomposition that has been discussed from thermodynamical analysis of the alloy.[22,23] Below the crystallization temperature, the only change detected by SWAXS measurements is this formation of very small solute clusters in glass. When the temperature reaches the crystallization temperature, T_x, a

strong scattering starts to appear at the q region lower than 2 nm^{-1} as shown in Fig. 3, suggesting the scattering contrast between the crystallites and the amorphous matrix gives another component of SAXS intensity. This component also shows power law of q^{-4} around 2 nm^{-1}, suggesting that the crystallites have rather sharp interface. When the cluster distribution is uniform inside the crystallites, the SAXS intensity of the model structure can be described by two components as,

$$I(q) = \{F_{cry}(q) + F_{cl}(q)\}\{F_{cry}(q) + F_{cl}(q)\}^* \quad (1)$$

where $F_{cry}(q)$ and $F_{cl}(q)$ denote the Fourier transform of the electron density contrast between inside / outside crystallites for $F_{cry}(q)$ and that between inside / outside clusters in the crystallites, where

$$I_{cry}(q) = F_{cry}(q)F_{cry}(q)^* \quad (2)$$

$$I_{cl}(q) = F_{cl}(q)F_{cl}(q)^* \quad (3)$$

The cross term, $I_{cross}(q) = F_{cry}(q)F_{cl}(q)^* + F_{cry}(q)^*F_{cl}(q)$, is negligible when the characteristic size of the crystals and clusters are different, i.e., the corresponding scatterings are observed at different q, which is the case for the present one. At higher temperatures above 520 K, $I_{cry}(q)$ decreased with increasing temperature, while the shoulder component observed for $I_{cl}(q)$ grew and eventually started to split into two peaks.

To examine the growth of the crystallites, SAXS components at the low-q region of $q<2$ nm^{-1} is extracted as $I_{cry}(q)$, using the Porod's law to separate the crystal component from the cluster component at larger q. For a detailed examination, the integrated intensity and the diameter of the crystallites obtained from $I_{cry}(q)$ are shown in Fig. 4. The integrated intensity for $I_{cry}(q)$ increased above T_x up to 525 K, corresponding to enhancement of contrast of the crystallites, suggesting some part of the solute segregates during coarsening of crystallites, i.e., during motion of the grain boundaries of crystallites. The integrated intensity then decreased above the temperature of 525 K. The size of the crystallites obtained from Guinier approximation grew from 6.8 nm at T_x to 16.2 nm at 610 K when the contrast of crystallites eventually vanished.

At the temperatures above 450 K, the shape of $I_{cl}(q)$ corresponding to the cluster components described above show a well-defined shoulder at q=5 nm^{-1} at 464 K as shown in Fig. 3 (a), for example, where the DSC curve suggests that the crystallization already completed. It is worthwhile noting that the SAXS pattern observed just after crystallization, i.e., the earliest microstructure formed in the crystalline phase is not a periodical concentration wave leading to the periodicity of structural/concentration modulation along c axis for 18R or 10H, but it is the scattering of clusters that distribute randomly in space[24]. To examine the developments of cluster structure, the SAXS

profile, $I_{cl}(q)$, were analyzed using a simplest scattering model of clusters approximated by ;

$$I_{cl}(q) = F^2(q) \cdot S(q) \quad (4)$$

where F(q) is the form factor, the Fourier transform of the shape of the particle, and S(q) is the structure factor that describes the spatial arrangements of the particles. Guinier approximation of the form factor gives the size of the cluster. Figure 5 gives the change of the average radius of the clusters. The cluster radius at the temperatures for relaxed glass was about 0.14 nm, corresponding to clusters containing a couple of atoms, and increase rapidly by 30 % upon crystallization. The cluster size increased to the size of the $L1_2$ cluster reported in the LPSO structures [15,16] at 560 K[24]. Iikubo et al.[22] showed that this process of cluster growth is below the spinodal temperatures, and therefore, thermodynamical analysis suggest spinodal nucleation[25] of the clusters. Knowing the cluster size, the spatial arrangements of cluster at the temperature is given by the structure factor, $S(q)$ taking the form factor of spherical particles with the radius of gyration obtained in Fig. 5. We analyzed $S(q)$ for the temperatures above 600 K assuming that the cluster size is that of Y_8Zn_6 clusters as defined in LPSO structures. Figure 6 shows the change of $S(q)$ during heating above the crystallization temperature. There are three important points to be noted in the figure, namely;

(1) At lower temperature below 550 K, $S(q)$ shows single peak profiles, meaning that there is only one characteristic cluster-cluster distance, i.e., spatial arrangements of cluster is isotropic in the initial stage of phase transformation.

(2) At higher temperatures between 550 K and 640 K, the peak splits into two peaks, one approaching to 4 nm^{-1} and the other to 6 nm^{-1}, corresponding to the periodicities of segregation layer for a LPSO structure and the inter-cluster distance within the segregation layer respectively. This means that the spatial arrangements of the clusters became anisotropic to form a cluster arrangement characteristic to the LPSO structures.

(3) At the temperatures above 640 K, such anisotropy continued to grow. At a closer examination, a sharp peak start to grow at 4.0 nm^{-1} from a diffuse peak whose peak lies between 4.2 nm^{-1} and 4.7 nm^{-1}, although the peak corresponding to the in-plane correlation at 6 nm^{-1} remained diffuse.

Therefore, the change of the SAXS profiles from single peak to double peak suggests that the spatial distribution of the clusters changes from isotropic distribution to anisotropic one, reflecting the LPSO structures. Concerning the formation mechanism of LPSO, an important question still left is when the stacking fault is introduced. The wide-angle X-ray diffraction (WAXD) profiles taken simultaneously with the SAXS data are shown in

Fig. 7. Before crystallization, the WAXD profiles showed a halo pattern typical for glass materials, and upon crystallization, well-defined Bragg peaks appeared. The peak was indexed as **0 1 3** Bragg peak from an hcp crystal. This peak does not appear for 18R structures, and start to decrease when introduction of stacking fault starts to occur toward formation of LPSO structure. Therefore, it is concluded that highly supersaturated hcp crystals form by crystallization, and the isotropic clusters grow in this hcp crystallites during early stage of annealing. A rapid decrease of hcp peak for WAXD and a splitting of the structure factor into two peaks at higher temperatures for SAS above 550 K means that introduction of stacking fault and anisotropic arrangement of clusters occur simultaneously. In contrast, the two sharp peaks marked by a solid asterisk appeared upon crystallization, and continued to grow with shifting the peak position, even after the hcp peak mentioned above diminished, and well-defined LPSO structure is observed by SAXS diffraction in Fig. 3(b). These peaks correspond to the ones where Bragg peaks for 18R, fcc, and hcp appear at almost the same angle. The Bragg peaks for 18R shown by double asterisks increased later, since the periodicity of the stacking faults, or the segregation periodicity, is not regular enough to give diffraction peaks for 18R in the early stage of structural transformation.

The formation sequence of the LPSO from amorphous ribbons during heating at a constant rate of 10 K/min. is schematically illustrated in Fig.8. (A) The amorphous ribbons contains very small solute clusters, which slightly grew upon relaxation. (B).Just after crystallization, the crystallites are small hcp crystals of about 7 nm in diameter, with isotropically distributed solute clusters in them. Segregation at grain boundary should be very small just after crystallization, since no apparent small angle scattering related to the grain size was observed. During crystal growth of hcp crystallites, clustering inside the crystallites also developed. Segregation at the grain boundary occured during the grain growth, which results in increase in the small-angle scattering intensity for crystallites as shown in Fig.3. (C)At higher temperatures above 550 K, the crystallites continued to grow. Anisotropic arrangements of clusters whose size reaches to that for $L1_2$ Y_8Zn_6 clusters, and introduction of stacking faults occurred simultaneously, which resulted in the splitting of a peak into two diffuse peaks corresponding to the in-plane and the out-of-plane LPSO cluster distances. The SAXS peaks for 18R appearing at about 4 nm^{-1} remain broad and larger than 4.0 nm^{-1} between 550 K and 640 K, suggesting that the LPSO structure transformed from isotropic clusters contained large amount of 'wrong' spacing. Coexistence of 18R and 10H LPSO has been observed during annealing Mg85Y9Zn6 cast alloy samples, where periodicity for 18R gives the peak at 4 nm^{-1} and that for 10H gives the peak at 4.8 nm-1[10,13] For

these microstructures, the peak positions for 10H and 18R are separated and they never changed with time. In contrast, the diffuse peak observed in the present case lies between them, suggesting that the periodicity should be regarded as a random mixture of every 6 layers (18R) and every 5 layers (10H), whose origin should be a random spatial arrangements of clusters in the early stage of phase transformation.

The SAXS contrast due to grain boundary segregation decreased and eventually vanished at this stage. (D) By further annealing at temperatures above 640 K, the structure factor in Fig.6 shows that a sharp peak at 4 nm^{-1} start to appear independently from the broad peak, suggesting that highly ordered 18R grains nucleated heterogeneously and grew into the defective 18R grains, which should be much more efficient transformation path to lead the microstructure into a more stable state than a sluggish rearrangements of periodicity by diffusion inside defective 18R grains, which requires diffusionand a motion of stacking faults.

Conclusions

In-situ SWAXS measurements of $Mg_{85}Y_9Zn_6$ ribbon rapidly quenched from liquid have been presented. Simultaneous measurements of SAXS and SWAXD revealed that:

(1) Supersaturated amorphous ribbon was obtained. Upon annealing, clustering of the solute atoms occurred even in the glass state.
(2) Just after crystallization, the small crystallites are hcp with strong supersaturation of Y and Zn, which is not realized by normal quenching of solid samples.
(3) Early stage of phase transformation is characterized by growth of solute clusters which distribute isotropically in hcp grains.
(4) When the size of cluster reached that for $L1_2$ clusters in LPSO, spatial distribution of clusters became anisotropic to form LPSO, with introduction of stacking faults.

Present work showed that the formation of LPSO at the 18R stoichiometry composition is characterized by two-step hierarchical phase transformations, the first step of spinodal nucleation of clusters, and the second step of spatial rearrangement of clusters accompanied by structural phase transformations.

Acknowledgments

Present work has been supported by Grant-in-Aid for scientific researches by MEXT/JSPS, numbers 23109005 and 26630294. SWAXS measurements have been performed under proposal numbers 2013G576, 2015G519 at Photon Factory and 2013B1383 and 2015A1448, 2015B1458 at Spring8.

References

1. Y.Kawamura,K.Hayashi,A.Inoue,T.Masumoto, Mater. Trans. 42(2001)1172.
2. T.Itoi, S.Simmya, Y.Kawmaura, M.Hiroshashi, Scripta Mater. 51(2004)107.
3. E. Abe A.Ono, T.Itoi, M.Yamasaki, Y.Kawamura, Philos. Mag., Lett., 91 (2011)690.
4. Y.M. Zhu, A.J.Morton, J.F. Nie, Acta Mater. 58 (2010)2936-2947.
5. H.Yokobayashi K.Kishida, H.Inui, M.Yamasaki, Y. Kawamura, Acta Mater. 59 (2012)7287.
6. D.Egusa, and E. Abe Acta Mater. 60 (2012)166-178.
7. G. Shao, V.Varsani Z.Fan, CALPHAD 30 (2006) 286-295.
8. S.Minamoto, S.Nemoto, A.Hayama, T.Horiuchi and S.Miura,ISIJ Intern. 50 (20**) 1914-1919.
9. J.Grobner, A.Kozlov, X.Y. Fang, J.Geng, J.F.Nie, R. Schmidt-Fetzer Acta Mater. 60(2012)5948-5.
10 H.Okuda, T.Horiuchi, T.Tsukamoto, S.Ochiai, M.Yamasaki and Y.Kawamura Scripta Mater. 75 (2014)66-69.
11..M.Yamasaki, M.Matsushita, K.Hagihara,K.Izuno,E.Abe, Scr. Materialia 78-79 (2014)13-16.
12.
13. H.Okuda, T.Horiuchi, T.Tsukamoto, S.Ochiai, M.Yamasaki and Y.Kawamura Scripta Mater. 68 (2013) 575-578
14. J.E.Saal and C.Wolverton, Acta Materialia 68(2014)325-338
15.. J.E.Saal, C.Wolverton, Scripta Materialia 67(2012)798-801.
16. H. Kimizuka, M. Fronzi, S.Ogata, Scripta Materialia 69 (2013) 594-597
17.. H.Kimizuka, S.Kurokawa, A.Yamaguchi, A.Sakai and S.Ogata Scientific Reports 4(2014)7318.
18. S.Kurokawa, A.Yamaguchi, amd A. Sakai :Mater. Trans. 54(2013)1073-1074.
19. K.Kishida, K.Nagai, A.Matsumoto, A.Yasuhara and H.Inui, Acta Mater. 99(2015)228-239.
20. H.Okuda T.Horiuchi, H.Tanaka, M. Yamasaki, Y.Kawamura and S. Kimura, Mater. Trans. 56(2015)906-909.
21.J.Cahn, Acta Metall.,9(1961)795-801.
22 S.Iikubo, S.Hamamoto and H.Ohtani Mater. Trans. 54(2013)636-640.
23. R. Matumoto, H.Ohtani and M.Hasebe, J. Jpn. Inst. Metals 73 (2009) 683-690.
24 H.Okuda, M.Yamasaki Y.Kawamura, M.Tabuchi, and H. Kimizuka, Scientific

Reports, 5 (2015)14186..

25. J .W.Cahn and J.E.Hilliard J. Chem. Phys. 31 (1959) 688-699.

Figures and Figure ca

Fig.1 Change of specific heat obtained by differential scanning calorimetry at a heating rate of 10K/min.

Fig.2 Schematic illustration of in-situ and simultaneous small- and wide- angle scattering/diffraction measurements.

Fig.3 Change of small-angle scattering for (a) around and (b) above Tx.

Fig.4 The diameter of the crystallites and the integrated intensity obtained for the SAXS intensity for the crystallites, $I_{cry}(q)$.

Fig.5 Change of average cluster radius during heating.

Fig.6 Change of the structure factors assuming form factors of spherical clusters with the size given in Fig.6. The plots are vertically shifted for visibility.

Fig.7 Change of Bragg peaks obtained by the WAXS detector during in-situ heating.
The peak shown by a broken line appears only when hcp stacking is assumed. The peaks shown by solid arrows appears when 18R stacking sequence is assumed.
The change of the integrated intensity of transient hcp peak is also shown in the inset.

Fig.8. Schematic explanation of phase transformation sequences obtained for the present alloy. Just after crystallization, the crystallites are small hcp ones containing clusters. At higher temperatures, crystallites and clusters grew, and the spatial arrangements of the clusters became anisotropic, with weak segregation at the grain boundary. Then the microstructure finally transformed into 18R structures. For (D), Mg atoms are not shown for clarity.

Figures and Figure captions.

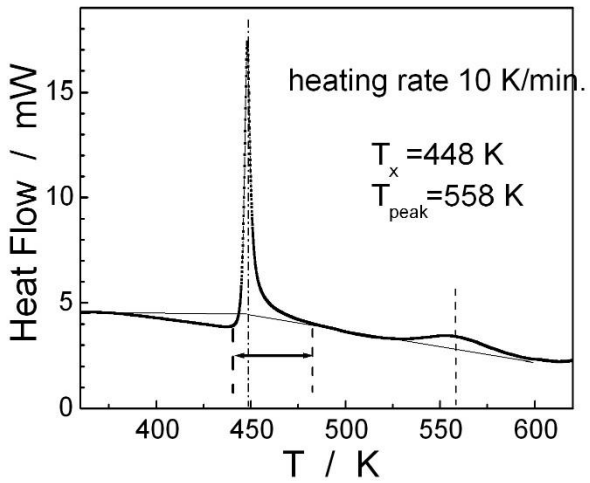

Fig.1 Change of specific heat obtained by differential scanning calorimetry at a heating rate of 10K/min.

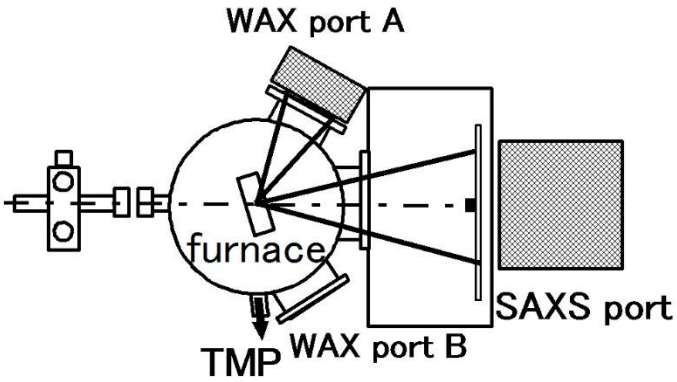

Fig.2 Schematic illustration of in-situ and simultaneous small- and wide- angle scattering/diffraction measurements.

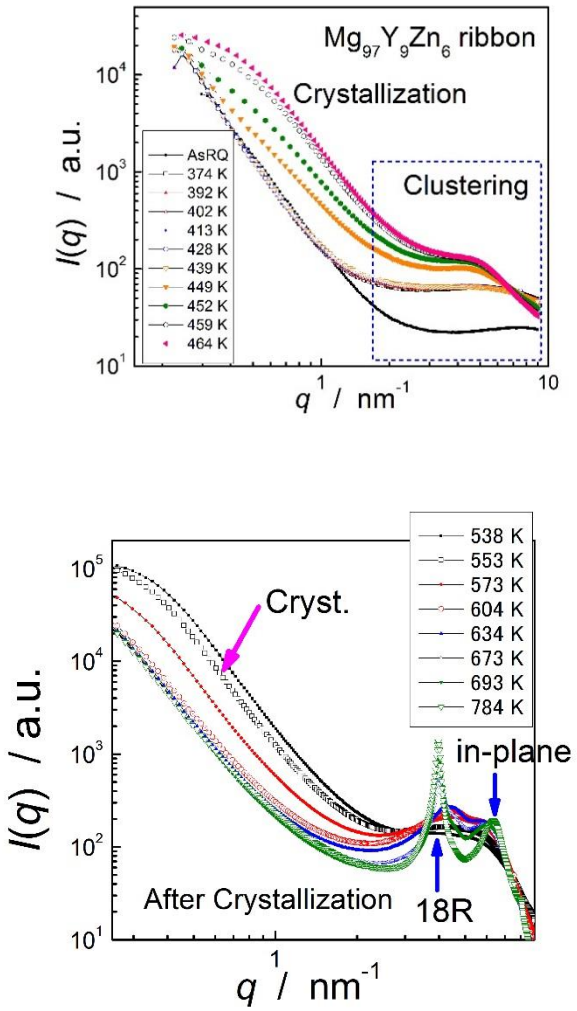

Fig.3 Change of small-angle scattering for (a) around and (b) above Tx.

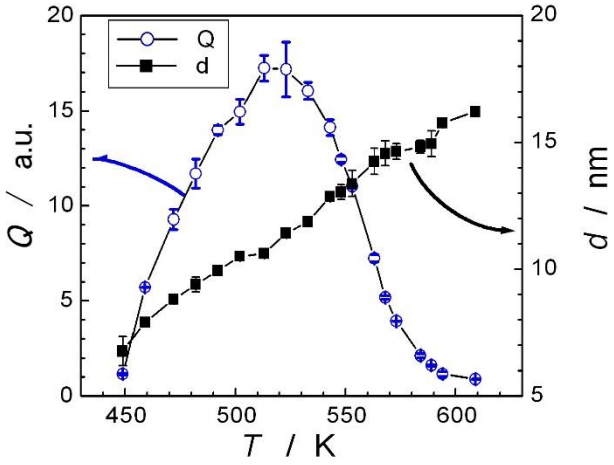

Fig.4 The diameter of the crystallites and the integrated intensity obtained for the SAXS intensity for the crystallites, $I_{cry}(q)$.

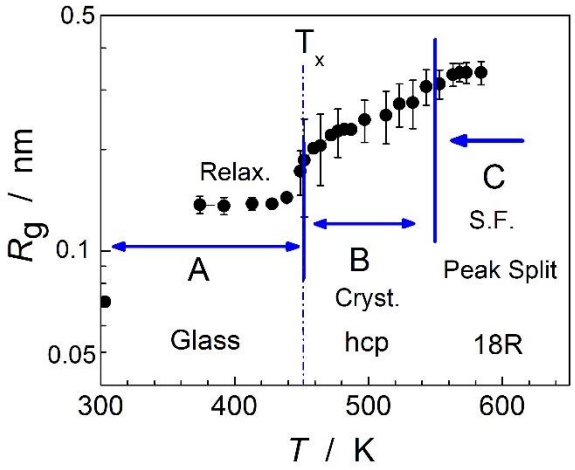

Fig.5 Change of average cluster radius during heating.

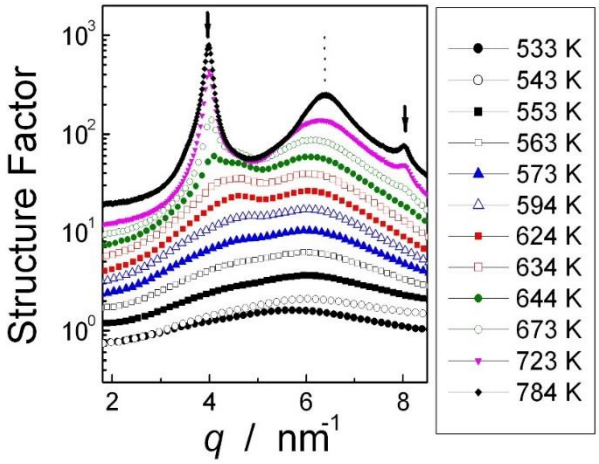

Fig.6 Change of the structure factors assuming form factors of spherical clusters with the size given in Fig.6. The plots are vertically shifted for visibility.

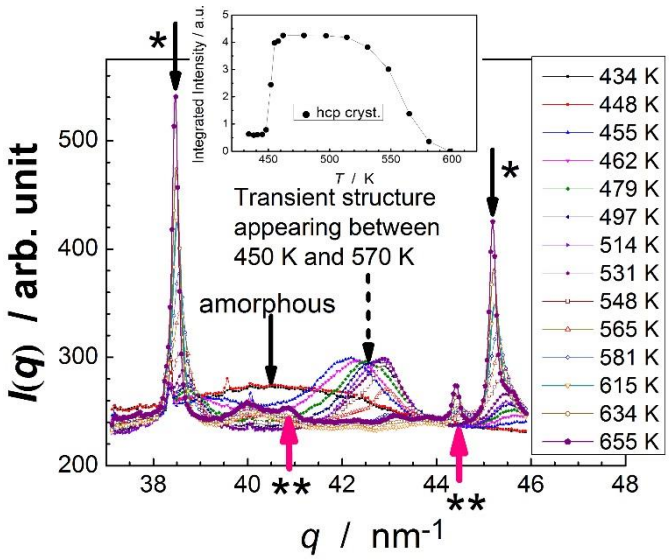

Fig.7 Change of Bragg peaks obtained by the WAXS detector during in-situ heating.
The peak shown by a broken line appears only when hcp stacking is assumed. The peaks shown by solid arrows appears when 18R stacking sequence is assumed. The change of the integrated intensity of transient hcp peak is also shown in the inset.

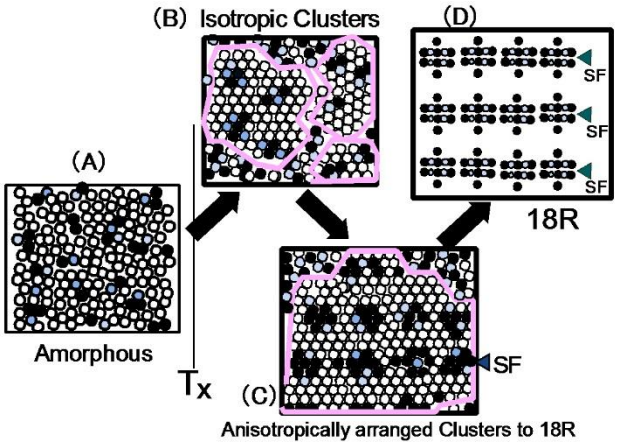

Fig.8. Schematic explanation of phase transformation sequences obtained for the present alloy. Just after crystallization, the crystallites are small hcp ones containing clusters. At higher temperatures, crystallites and clusters grew, and the spatial arrangements of the clusters became anisotropic, with weak segregation at the grain boundary. Then the microstructure finally transformed into 18R structures. For (D), Mg atoms are not shown for clarity.